

Supplementary Information

for

Defect-induced electric field effects direct Fenton-like oxidation pathways towards polymerization for sustainable water treatment

Banghai Liu^a, Changkun Yang^a, Xinpeng Huang^a, Yin Pan^b, Cheng Cheng^a, Wanqian

Guo^c, Liyuan Liang^d, Zhenyu Wang^a, Feng He^{a*}

^aInstitute of Environmental Processes and Pollution Control, and School of
Environment and Ecology, Jiangnan University, Wuxi 214122, China

^bCollege of Environment, Zhejiang University of Technology, Hangzhou 310014,
China

^cState Key Laboratory of Urban Water Resource and Environment, Harbin Institute of
Technology, Harbin 150090, China

^dDepartment of Earth and Planetary Sciences, University of Tennessee, Knoxville, TN
37996, United States

*Corresponding author: Feng He

Email address: fenghe@jiangnan.edu.cn (F.H.)

Number of pages: 37, Number of figures: 22, Number of tables: 6

Text S1. Chemicals and Reagents

Industrial grade multi-wall carbon nanotubes (96%), melamine (99%), dicyanodiamine (99%), PMS (available as Oxone®, $\text{KHSO}_5 \cdot 0.5\text{KHSO}_4 \cdot 0.5\text{K}_2\text{SO}_4$), sodium carbonate (NaHCO_3 , AR), sodium chloride (NaCl , AR), sodium sulfate (NaSO_4 , AR), sodium nitrate (NaNO_3 , AR), sodium hydroxide (NaOH , AR), 5,5-dimethyl-1-pyrroline N-oxide (DMPO), 2,2,6,6-tetramethyl-4-piperidinol (TEMP), acetonitrile, and 2,6-dimethylphenol (2,6-M-PhOH) were purchased from Sigma–Aldrich. Potassium iodide (KI, 99%), *tert*-butanol (*t*-BuOH, 99%), and methanol (MeOH, 99%), were supplied by Sinopharm Chemical Reagent Co., Ltd. Phenol ($\text{C}_6\text{H}_6\text{O}$, AR), *p*-chlorophenol ($\text{C}_6\text{H}_5\text{ClO}$, AR), and urea ($\text{CH}_4\text{N}_2\text{O}$, 99%) was purchased from Shanghai Macklin biochemical technology Co., Ltd. All chemical reagents were used without further purification.

Text S2. Electrochemical measurements and Degradation product identification.

The surface elemental content of the catalysts was analyzed by X-ray photoelectron spectroscopy (XPS, ESCALab 250Xi, Thermo Fisher) at Al $\text{K}\alpha$ radiation of 1486.6 eV. X-ray diffraction (XRD) patterns were performed on an X-ray diffractometer (Bruker D8 Advance Davinci, Germany) with a Cu $\text{K}\alpha$ radiation source ($\lambda=0.154$ nm). Transmission electron microscopy (TEM) was used to observe the morphology and structure of the sample. Raman spectroscopy was collected from a confocal LabRAM HR Evolution (Horiba, France) spectrometer with a laser at 532 nm. The suspensions obtained at a given time were filtered through PTFE and then analyzed by a TOC-VHP analyzer (SSM-5000A, Japan) for the determination of total organic carbon (TOC). EPR measurements (Bruker A300 EPR spectrometer, Germany) were carried out with 2,2,6,6-tetramethyl-4-piperidinol (TEMP) or 5,5-dimethyl-1-pyrroline N-oxide (DMPO) as a spin trapping agent. Detailed information for electrochemical

tests and polymer analytical methods can be found in SI-[Text S2](#).

Electrochemical measurements

The electrochemical electrode was prepared by homogeneously mixing 50 mg CNTs samples, 0.25 mL Nafion solution (5 wt %), 2.5 mL acetonitrile, and 2.5 mL deionized water. The mixture was then ultra-sonicated for 3 h. Then, 2.5 μ L suspension was dropped onto pre-cut carbon paper (about 1 cm²) and dried at 40°C for 5-6 min. All electrochemical measurements were performed in a traditional three-electrode configuration using silver/silver chloride electrode (Ag/AgCl) and Pt ring electrode as reference and counter electrode. A CHI760E electrochemical workstation was used for related tests, namely, electrochemical impedance spectroscopy (EIS) and chronoamperometric. EIS was measured at 0.75 V (vs. Ag/AgCl) from 100,000 to 1 Hz in O₂-saturated 0.1 M KOH solution. Chronoamperometries were conducted at an applied potential of 0.6 V using 100 mM phosphate buffer as solution. With the addition of aliquots of PMS and 4-CP, the current change was monitored immediately.

Degradation product identification.

The reaction system was enlarged by a factor of 5 to collect degradation products better. After 90 minutes of reaction, the catalyst was collected by vacuum filtration. The products attached to the catalyst surface were sequentially eluted using ethanol and toluene to obtain eluent A and eluent B, respectively.

LC-MS: Oxidation products dissolved in eluent A were analyzed using liquid chromatography-mass spectrometry (LC-MS, SYNAPT G2-Si, Waters, USA) equipped with an HPLC system and an electron spray ionization source under negative ionization mode.

GPC: The brown soft solid obtained after drying of eluate B was redissolved in tetrahydrofuran (THF), and the molecular mass of the dissolved product was further

determined by gel permeation chromatography (GPC, LC-20ADXR, Shimadzu, Japan) at 40 °C.

MALDI-TOF-MS: The brown soft solid obtained after drying of eluate B was redissolved in tetrahydrofuran. The obtained solution was further mixed homogeneously with matrices (2,5-dihydroxybenzoic acid, DHBs). Subsequently, matrix-assisted laser desorption/ionization mass spectrometry (MALDI-TOF MS; ultraflexXtreme, Bruker, USA) was used to record the properties of the products dissolved in THF under negative ionization mode.

FTIR: The brown soft solid obtained after drying of eluate B was analyzed by Fourier transform infrared spectroscopy (FTIR, INVENIO S, Bruker, USA) in the wavenumber range from 400 to 3600 cm⁻¹.

Text S3. Computational methods.

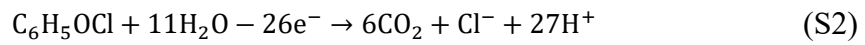
The neutral carbon-based cluster models were created by Gauss view 5.0.8 with H atoms terminating the dangling bonds of the edge atoms. All DFT calculations in this work were carried out in Gaussian 09 package (Revision D.01). The geometry optimizations and vibrational frequency calculations were performed at B3LYP/6-311G (d, p) level. Single point energy of the optimized geometry was calculated at B3LYP/6-311+G (d, p) level in view of dispersion correction. The adsorption energy of PMS on carbon-based cluster was calculated based on: $E_{\text{ads}} = E_{\text{complex}} - E_{\text{surface}} - E_{\text{PMS}}$, where E_{complex} refers to the single point energy of adsorption complex, while E_{surface} and E_{PMS} represent the energy of isolated molecule and the carbon surface, respectively. Electrostatic potential (ESP) distributions, valence-electron density, independent gradient model based on Hirshfeld partition, and local electron attachment energy (LEAE) were conducted with the Multiwfn software and graphed with VMD¹.

Text S4. Calculation of electron utilization efficiency.

As previously reported²⁻⁴, the electron utilization efficiency (EUE) is defined in this study as the ratio of the electron equivalents given by the reductant (organic pollutant) ($n_{given\ e^-}$, mol) to the electron equivalents obtained by the oxidant ($n_{obtain\ e^-}$, mol), as shown in Equation (S1):

$$EUE = \frac{n_{given\ e^-}}{n_{obtain\ e^-}} \times 100\% \quad (S1)$$

The value of $n_{given\ e^-}$ is calculated from the mineralization rate of the organic pollutant. Taking [4-CP] = 0.5 mM as an example, the given e^- = [4-CP] × TOC removal × 26 = 0.5 × 74.79% × 26 = 9.732 mM (S2).



The value of $n_{obtain\ e^-}$ is calculated based on the actual consumption of the oxidant. One mole of persulfate (peroxymonosulfate (PMS) and peroxydisulfate (PDS)) molecules obtains two moles of electrons during activation. Taking [PMS]_{initial} = 1.0 mM as an example, the obtained e^- = [PMS]_{actual} × 2 = 0.881 × 2 = 1.763 mM. The actual consumption of PMS/PDS (i.e., 0.881 mM) was detected and calculated using the UV spectrophotometric method at 352 nm.

Text S5. Internal electric field analysis.

The magnitudes of the interfacial electric field in CNTs are calculated through macroscopic characterization^{5,6}. The intensity of the interfacial electric field (IEF) is determined by surface potential and surface charge density, as follows:

$$E = \frac{-2V_s\rho}{\varepsilon\varepsilon_0} \quad (S3)$$

Where E is the IEF magnitude, V_s is the surface potential, ρ is the surface charge density, ε is the low-frequency dielectric constant, and ε_0 is the vacuum dielectric constant. The V_s is obtained by AFM in surface potential mode. The ρ is determined by zeta potential and then calculated using the Gouy-Chapman model, as follows:

$$\sigma = \sqrt{8kT\varepsilon\varepsilon_0n} \sinh\left(\frac{ze_0\psi_0}{2kT}\right) \quad (S4)$$

Where σ is surface charge density, k is the Boltzmann constant, T is absolute temperature, ε is relative medium constant, ε_0 is vacuum dielectric constant, n is vacuum dielectric constant, z is electrolyte valence, e_0 is the electron charge, ψ_0 is the surface potential.

Text S6. Construction of M-DCNT/PVDF composite microfiltration membrane.

We constructed an M-DCNT/polyvinylidene fluoride (PVDF) composite microfiltration membrane system through vacuum filtration⁷. In brief, 50 mg of M-DCNT catalyst was dispersed in 200 ml of ultrapure water by 30 min of sonication. The M-DCNT suspension was then gradually deposited (in small amounts and multiple times) on the surface of the PVDF membrane by direct vacuum filtration.

Table S1. Operation parameters for organic contaminant analysis with HPLC.

organic contaminants	mobile phase				detection wavelength (nm)	flow rate (mL/min)
	water	Acetonitrile (%)	Water (%)	Methanol (%)		
	(0.1% formic acid)					
Phenol			40	60	280	1.0
4-CP			40	60	280	1.0

Table S2. BET structural parameters of different CNTs.

Sample	S _{BET} (m ² /g)	Pore volume (cm ³ /g)	Pore size (nm)
CNT	183.212	0.864	16.911
M-CNT ^{bm*}	38.881	0.503	44.412
D-CNT ^{bm}	35.851	0.041	37.719
U-CNT ^{bm}	33.132	0.181	18.123
M-DCNT	348.123	1.507	12.584
D-DCNT	317.837	0.935	10.984
U-DCNT	288.113	0.736	9.419

* ^{bm} denoted as ball mill

Table S3. Elemental composition of different CNTs by XPS

Sample	C (at.%)	O (at.%)	N (at.%)
CNT	97.45	1.85	0.51
M-CNT ^{bm*}	67.41	4.41	28.18
D-CNT ^{bm}	65.26	6.83	27.91
U-CNT ^{bm}	87.06	9.19	3.76
M-DCNT	92.08	6.58	1.04
D-DCNT	94.91	3.01	2.08
U-DCNT	95.70	3.17	1.13

* ^{bm} denoted as ball mill

Table S4. Real surface water and groundwater quality detection parameters.

Parameters	surface water ^a	groundwater ^b
pH	7.10	7.82
COD (mg/L)	128	146
Conductivity (μS)	628	506
NH ₃ -N (mg/L)	0.50	2.86
NO ₃ ⁻ (mg/L)	0.69	2.06
PO ₄ ³⁻ (mg/L)	0.14	4.86
Cl ⁻ (mg/L)	145.69	41.57
SO ₄ ²⁻ (mg/L)	26.82	9.52

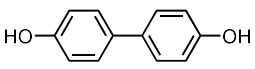
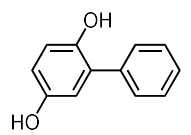
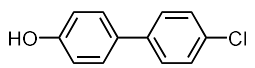
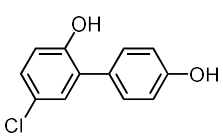
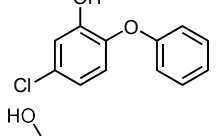
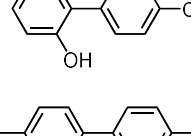
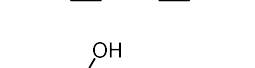
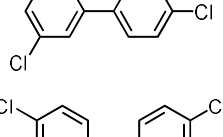
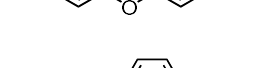
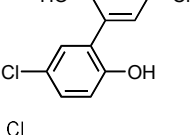
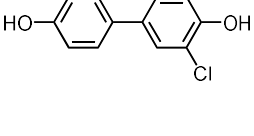
^a surface water from the lake within the Moganshan Campus of Zhejiang University of Technology

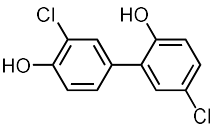
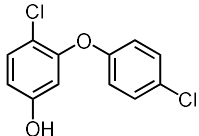
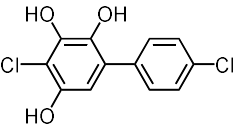
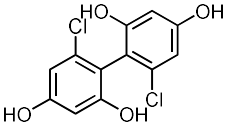
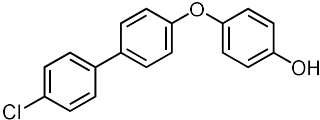
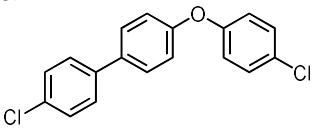
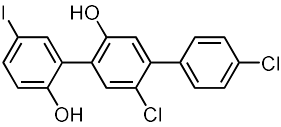
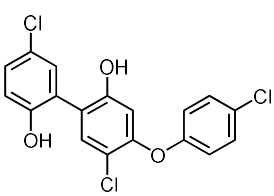
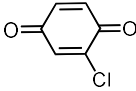
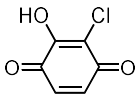
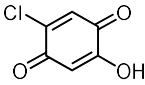
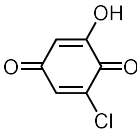
^b underground water from the ancient well in Ziyang Street, Hangzhou City

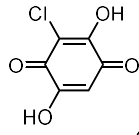
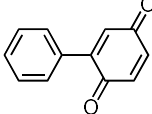
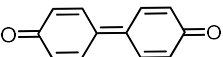
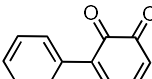
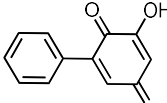
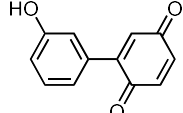
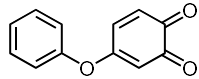
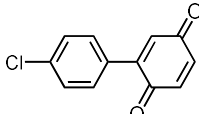
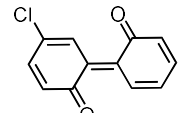
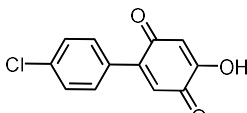
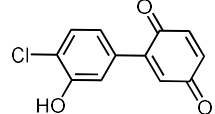
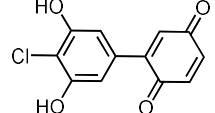

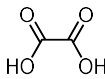
Table S5. Comparison of electron utilization efficiency of different systems.

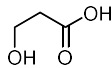
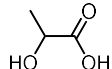
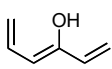
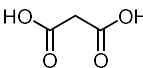
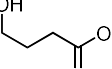
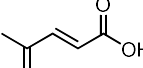
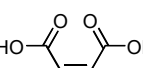
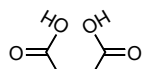
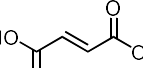
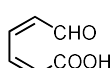
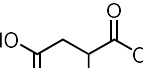
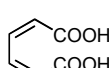
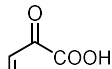
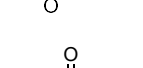
Catalyst (g L ⁻¹)	Oxidant (mM)	Pollutant (mM)	TOC removal (%)	Actual oxidant consumption (mM)	Given e^- (mM)	Obtained e^- (mM)	e^- utilization efficiency (%)	Ref.
Mn _{1.8} Fe _{1.2} O ₄ (0.1)	PMS (0.876)	BPA (0.044)	80.00%	0.651	2.534	1.302	194.62%	8
Mn ₂ O ₃ @Mn ₅ O ₈ (0.3)	PMS (1.500)	4-CP (0.623)	81.00%	1.500	13.120	3.000	437.33%	9
HEAs (0.1)	PMS (0.250)	BPA (0.044)	38.11%	0.250	1.067	0.500	213.42%	10
NG (0.1)	PMS (0.250)	PhOH (0.100)	33.43%	0.250	0.734	0.500	146.75%	10
Biochar-600 (0.1)	PMS (0.438)	BPA (0.044)	80.00%	0.326	2.534	0.652	388.65%	11
RSBC (0.6)	PMS (0.394)	Aniline (0.107)	52.00%	0.378	1.639	0.756	216.80%	12
BC800 (0.2)	PDS (0.100)	2,4,6-TCP (0.025)	77.00%	0.100	0.363	0.200	181.26%	3
CNTs (0.1)	PDS (0.031)	2,4-DCP (0.031)	40.00%	0.031	0.167	0.062	269.35%	13
M-DCNT (0.1)	PMS (1.000)	4-CP (0.500)	74.79%	0.881	9.723	1.763	551.58%	This work

Table S6. Information of the main products of 4-CP oxidation from LC-MS analysis in M-DCNT/PMS.

Formula	m/z	Retention time (min)	Proposed structure
Oligomers			
C ₁₂ H ₁₀ O ₂	185.0608	5.046	
C ₁₂ H ₁₀ O ₂	185.0608	5.109	
C ₁₂ H ₉ ClO	203.0269	5.241	
C ₁₂ H ₉ ClO ₂	219.0218	0.820	
C ₁₂ H ₉ ClO ₂	219.0218	5.427	
C ₁₂ H ₉ ClO ₂	219.0218	5.444	
C ₁₂ H ₈ Cl ₂	220.9930	5.195	
C ₁₂ H ₈ Cl ₂ O	236.9879	5.513	
C ₁₂ H ₈ Cl ₂ O	236.9879	5.380	
C ₁₂ H ₈ Cl ₂ O ₂	252.9829	2.242	
C ₁₂ H ₈ Cl ₂ O ₂	252.9829	4.271	

$C_{12}H_8Cl_2O_2$	252.9829	5.780	
$C_{12}H_8Cl_2O_2$	252.9829	6.387	
$C_{12}H_8Cl_2O_3$	268.9778	2.981	
$C_{12}H_8Cl_2O_4$	284.9727	5.913	
$C_{18}H_{13}ClO_2$	295.0531	5.329	
$C_{18}H_{12}Cl_2O$	313.0192	0.733	
$C_{18}H_{11}Cl_3O_2$	362.9752	0.716	
$C_{18}H_{11}Cl_3O_3$	378.9701	0.750	
Quinones			
$C_6H_3ClO_2$	140.9749	4.374	
$C_6H_3ClO_3$	156.9698	2.363	
$C_6H_3ClO_3$	156.9698	4.675	
$C_6H_3ClO_3$	156.9698	5.310	

$C_6H_3ClO_4$	172.9647	4.235	
$C_{12}H_8O_2$	183.0452	4.235	
$C_{12}H_8O_2$	183.0452	4.322	
$C_{12}H_8O_2$	183.0452	5.593	
$C_{12}H_8O_3$	199.0401	3.519	
$C_{12}H_8O_3$	199.0401	3.837	
$C_{12}H_8O_3$	199.0401	4.906	
$C_{12}H_7ClO_2$	217.0062	4.992	
$C_{12}H_7ClO_2$	217.0062	5.848	
$C_{12}H_7ClO_3$	233.0011	4.825	
$C_{12}H_7ClO_3$	233.0011	5.328	
$C_{12}H_7ClO_4$	248.996	4.825	
Organic acids			
$C_3H_8O_2$	75.0452	4.102	
$C_2H_2O_4$	88.988	0.802	

$C_3H_6O_3$	89.0244	2.178	
$C_3H_6O_3$	89.0244	3.952	
C_6H_8O	97.0659	1.473	
$C_3H_4O_4$	103.0037	4.755	
$C_4H_8O_3$	103.0401	5.160	
$C_5H_6O_3$	113.0244	0.837	
$C_4H_4O_4$	115.0037	0.820	
$C_4H_4O_4$	115.0037	5.160	
$C_4H_4O_4$	115.0037	5.460	
$C_6H_6O_3$	125.0244	4.287	
$C_4H_6O_5$	133.0142	5.258	
$C_6H_6O_4$	141.0193	5.091	
$C_6H_4O_6$	170.9935	3.449	
$C_6H_3ClO_6$	204.9545	8.194	

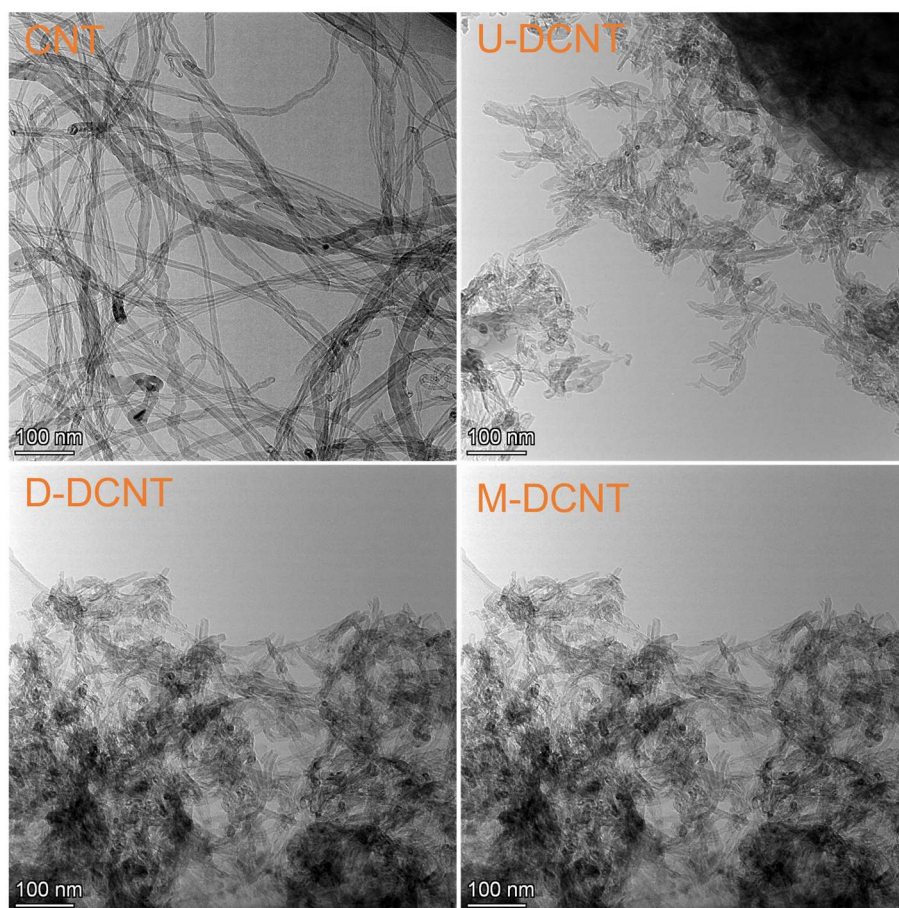


Figure S1. TEM images of CNT (a), U-DCNT (b), D-DCNT (c), and M-DCNT (d).

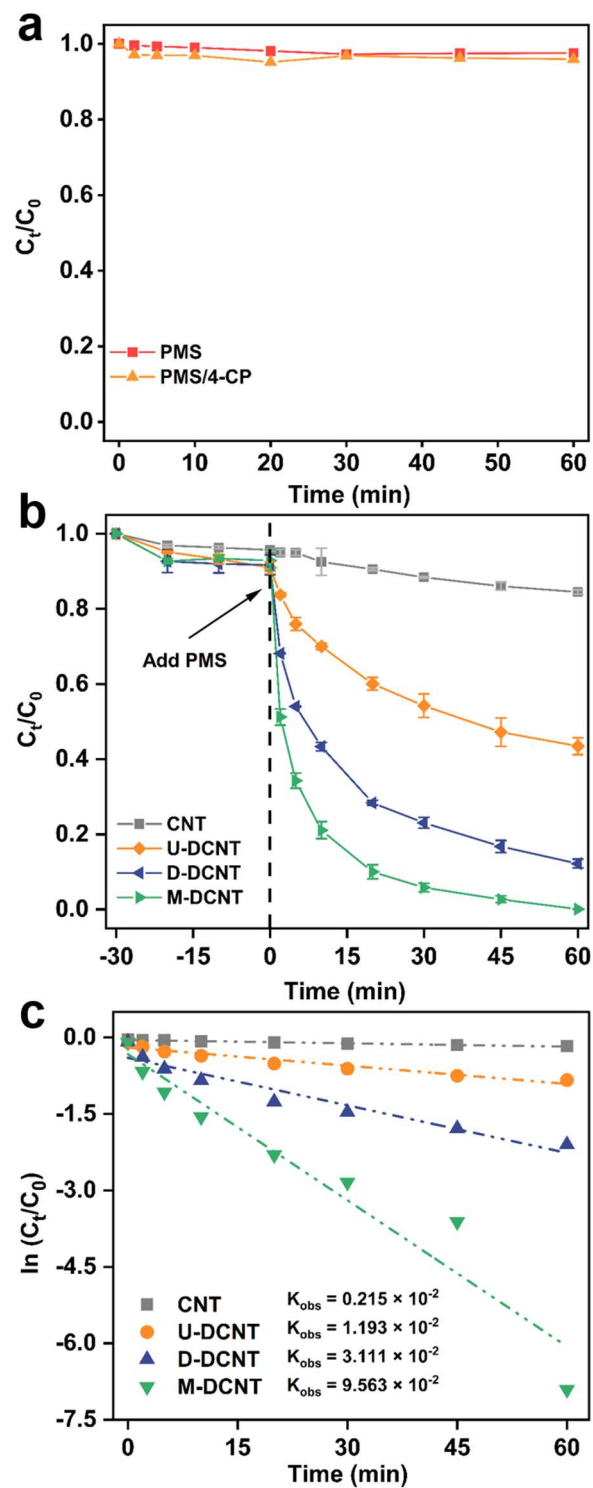


Figure S2. (a) Removal of 4-CP by PMS oxidation alone. (b) Removal of 4-CP in the (D)CNTs/PMS system. (c) Pseudo-first-order kinetic fitting for 4-CP removal. Reaction conditions: [Cat.] = 0.1 g L⁻¹, [PMS] = 1.0 mM, [4-CP] = 0.5 mM, initial pH = 7.4, and $T = 25 \pm 2^\circ\text{C}$. The error bars represent the standard deviations from duplicate or triplicate tests.

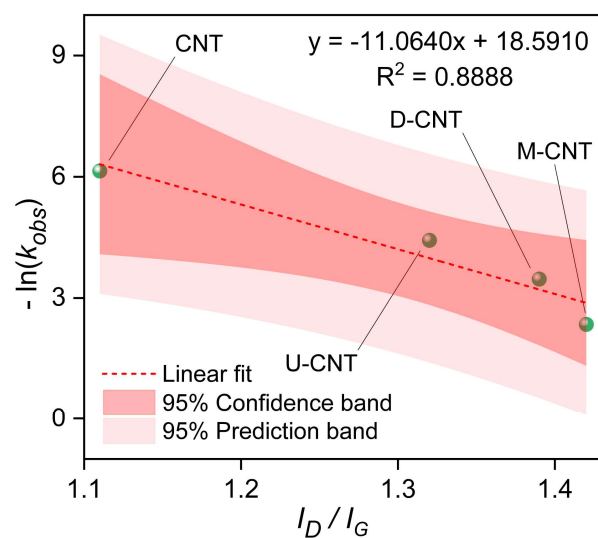


Figure S3. Correlation analysis between I_D/I_G and k_{obs} of the DCNTs. Reaction conditions: [Cat.] = 0.1 g L⁻¹, [PMS] = 1.0 mM, [4-CP] = 0.5 mM, initial pH = 7.4, and $T = 25 \pm 2^\circ\text{C}$.

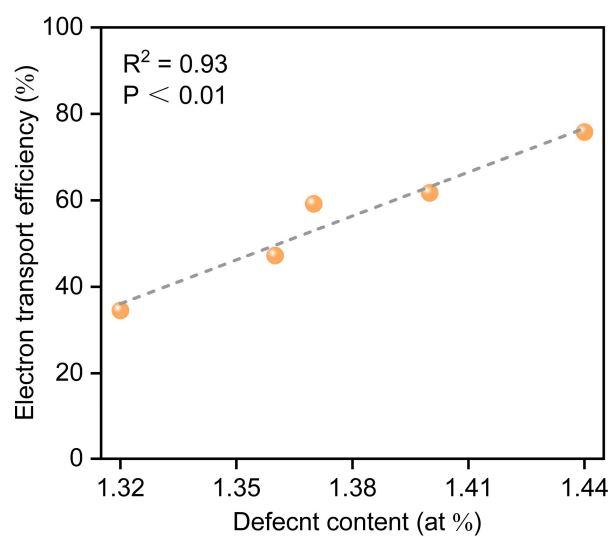


Figure S4. Correlation analysis between the defect degree of carbon catalyst treated at different annealing temperatures (500-800 °C) and electron transport efficiency.

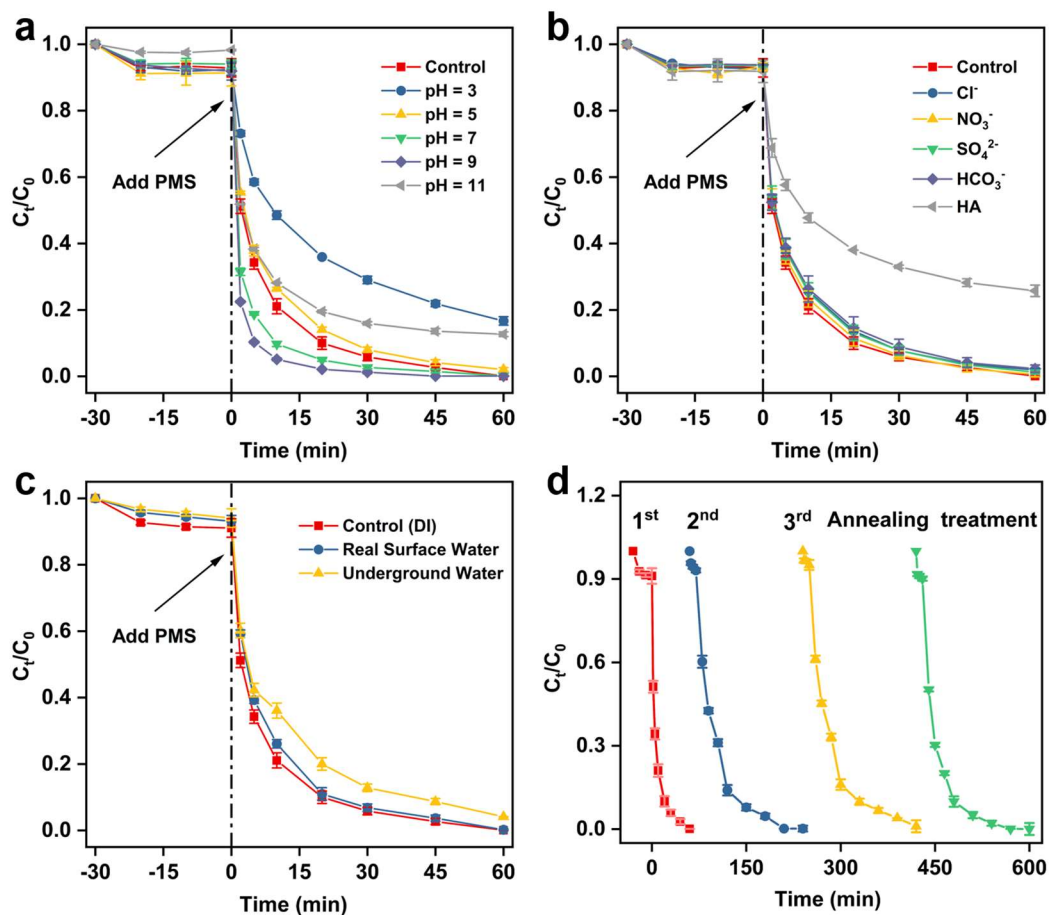


Figure S5. Effect of initial pH (a), anions (Cl^- , SO_4^{2-} , NO_3^- , HCO_3^-) and humic acid (HA) (b), water source (c) on the removal of 4-CP by PMS/M-DCNT. Stability tests of M-DCNT (d). Reaction conditions: $[\text{M-DCNT}] = 0.1 \text{ g L}^{-1}$, $[\text{PMS}] = 1.0 \text{ mM}$, $[\text{4-CP}] = 0.5 \text{ mM}$, $[\text{Cl}^-] = [\text{SO}_4^{2-}] = [\text{NO}_3^-] = [\text{HCO}_3^-] = 10 \text{ mM}$, and $[\text{HA}] = 10 \text{ ppm}$, initial pH = 7.4, and $T = 25 \pm 2^\circ\text{C}$. The error bars represent the standard deviations from duplicate or triplicate tests.

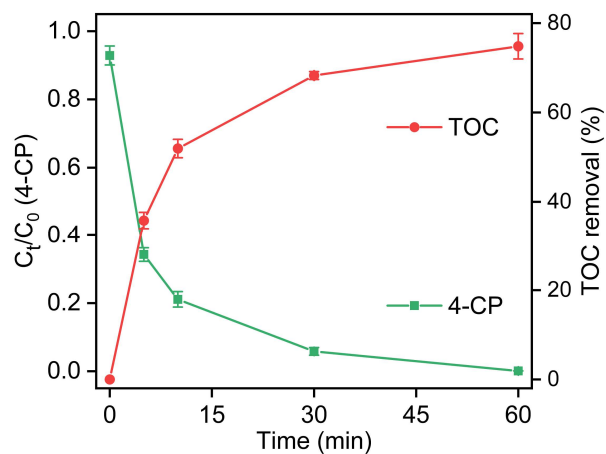


Figure S6. Removal of 4-CP and production of TOC by PMS/M-DCNT in DI water. Reaction conditions: $[M-DCNT] = 0.1 \text{ g L}^{-1}$, $[PMS] = 1.0 \text{ mM}$, and $[4-CP] = 0.5 \text{ mM}$, initial $\text{pH} = 7.4$, and $T = 25 \pm 2^\circ\text{C}$. The error bars represent the standard deviations from duplicate or triplicate tests.

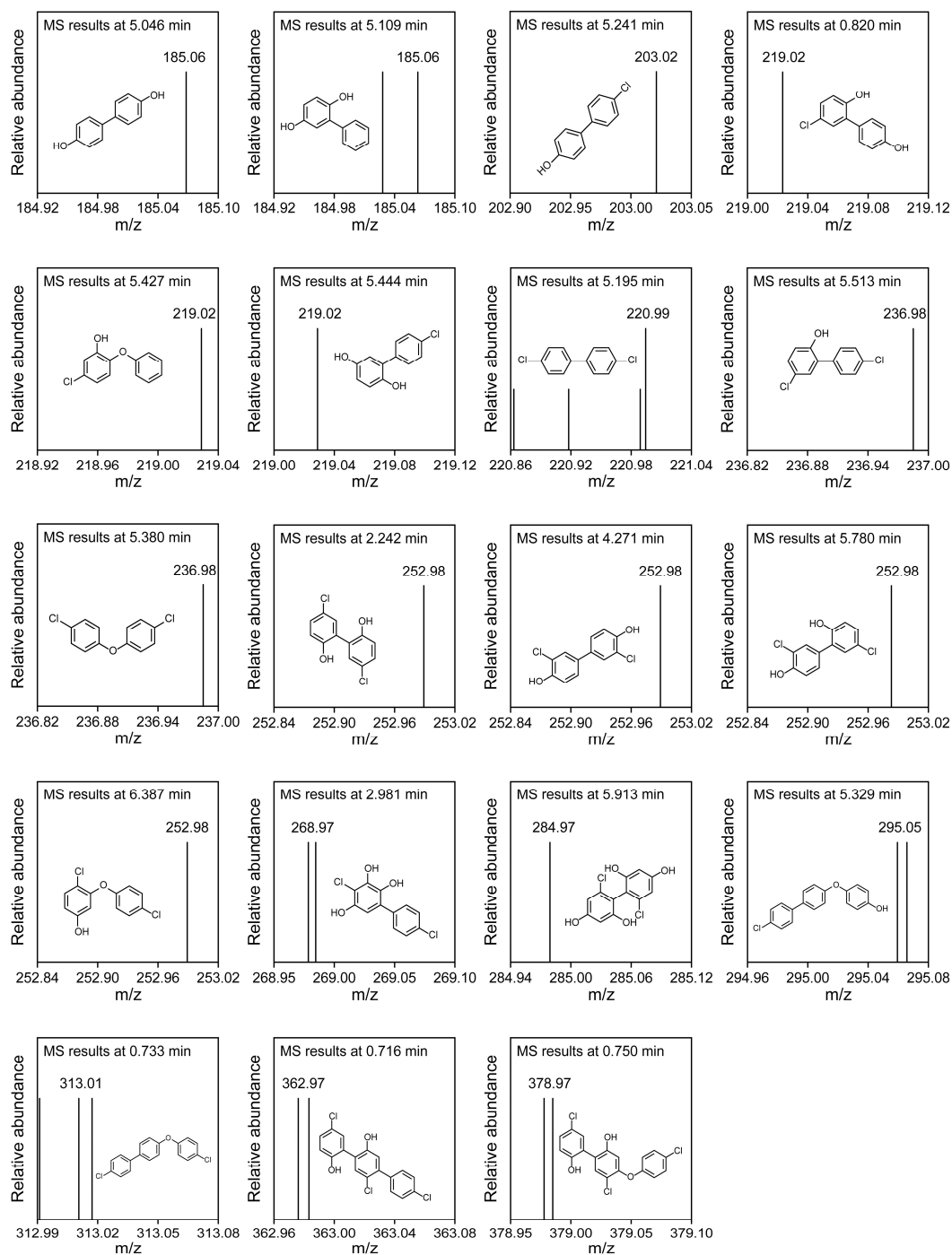


Figure S7. The LC-MS spectra of oligomer products detected in M-DCNT/PMS.

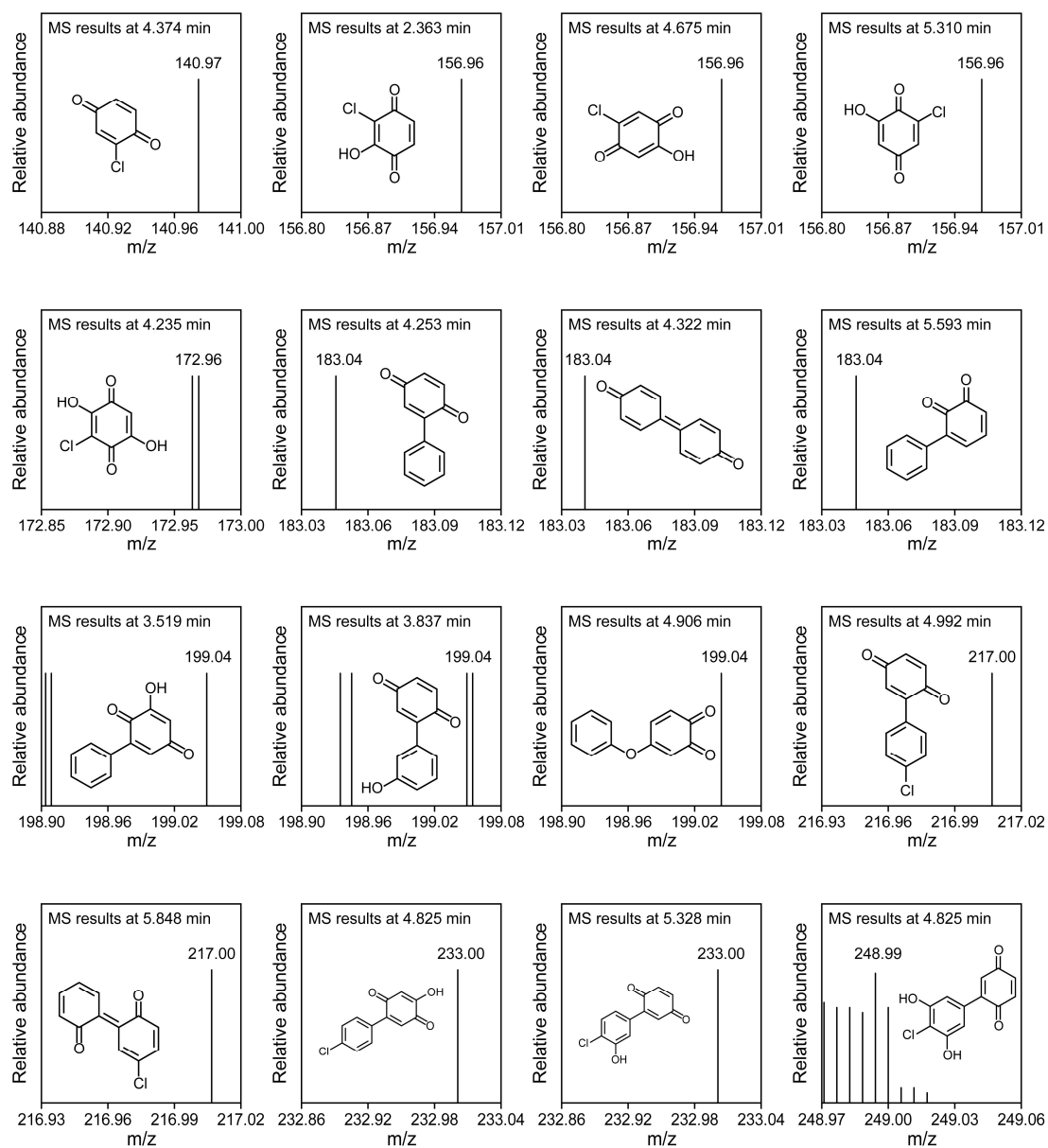


Figure S8. The LC-MS spectra of quinone products in M-DCNT/PMS.

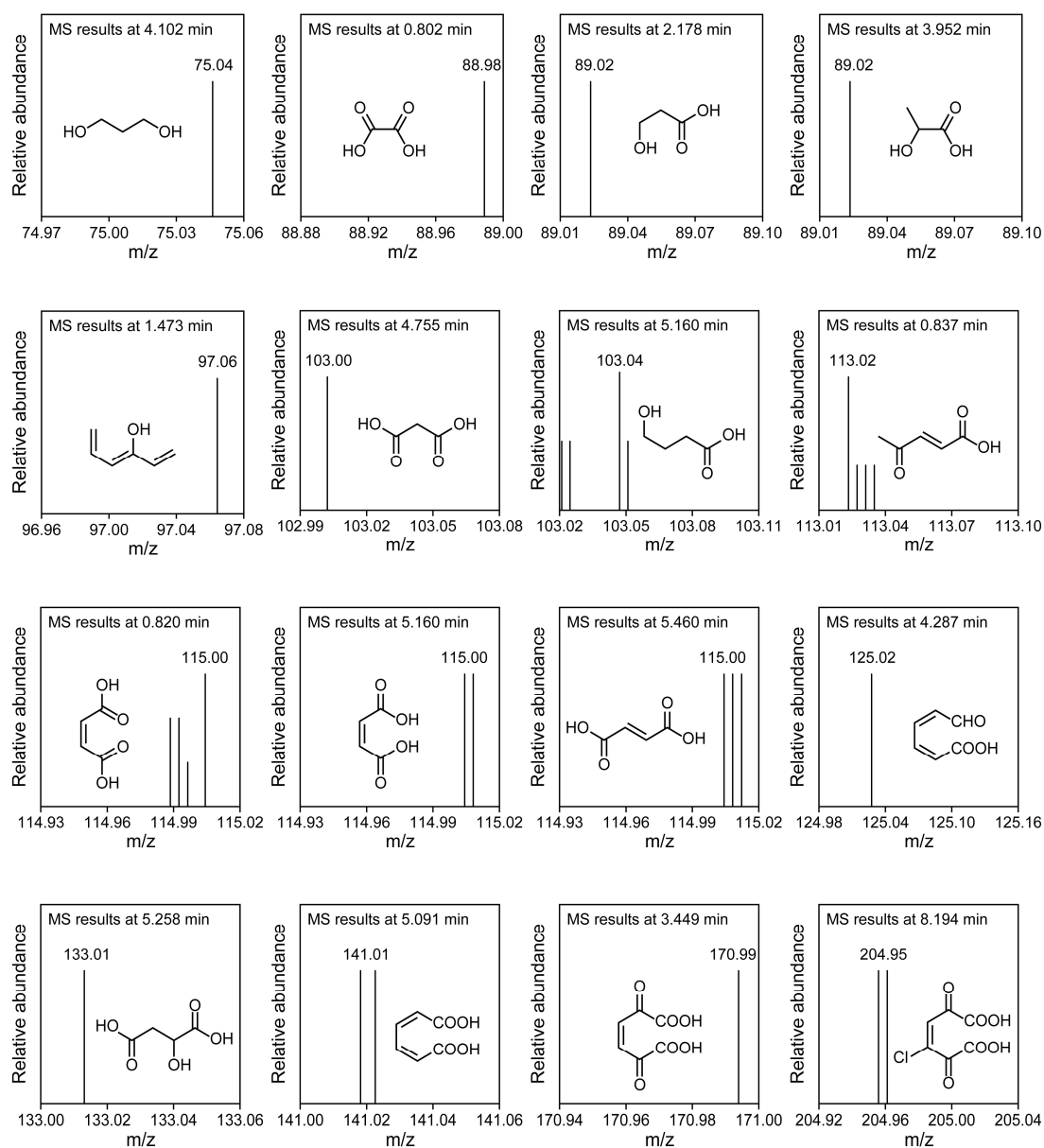


Figure S9. The LC-MS spectra of organic acids detected in M-DCNT/PMS.

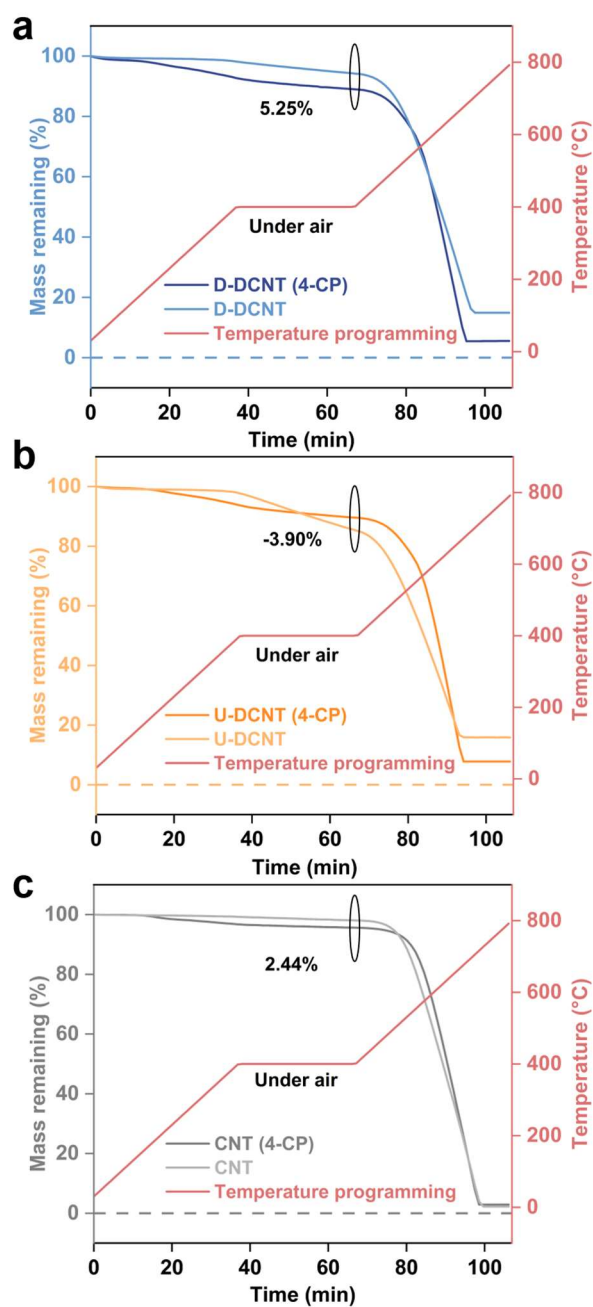


Figure S10. TGA curves of D-DCNT (a), U-DCNT (b), and CNT (c) before and after the reaction. Reaction conditions: [Cat.] = 0.1 g L⁻¹, [PMS] = 1.0 mM, [4-CP] = 0.5 mM, initial pH = 7.4, and $T = 25 \pm 2^\circ\text{C}$.

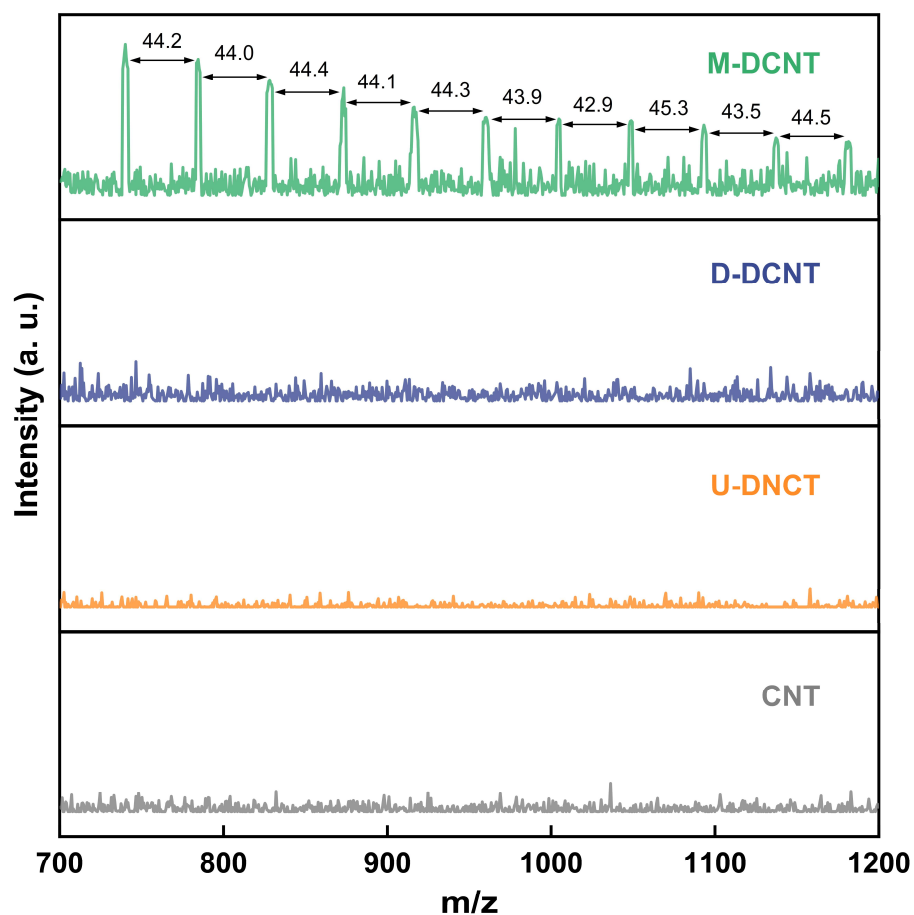


Figure S11. MALDI-TOF-MS spectra of polymerization products extracted from M-DCNT, D-DCNT, U-DCNT, and CNT surfaces. Reaction conditions: [Cat.] = 0.1 g L⁻¹, [PMS] = 1.0 mM, [4-CP] = 0.5 mM, initial pH = 7.4, and $T = 25 \pm 2^\circ\text{C}$.

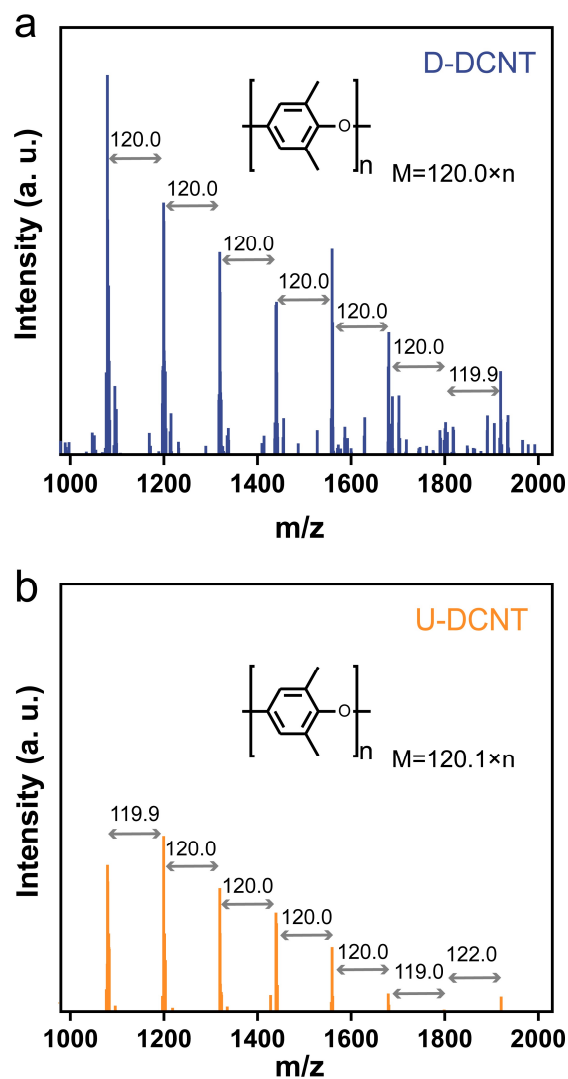


Figure S12. MALDI-TOF-MS spectra of polymerization products extracted from D-DCNT (a) and U-DCNT (b) surfaces. Reaction conditions: [Cat.] = 0.1 g L⁻¹, [PMS] = 1.0 mM, [2,6-M-PhOH] = 0.5 mM, initial pH = 7.4, and $T = 25 \pm 2^\circ\text{C}$.

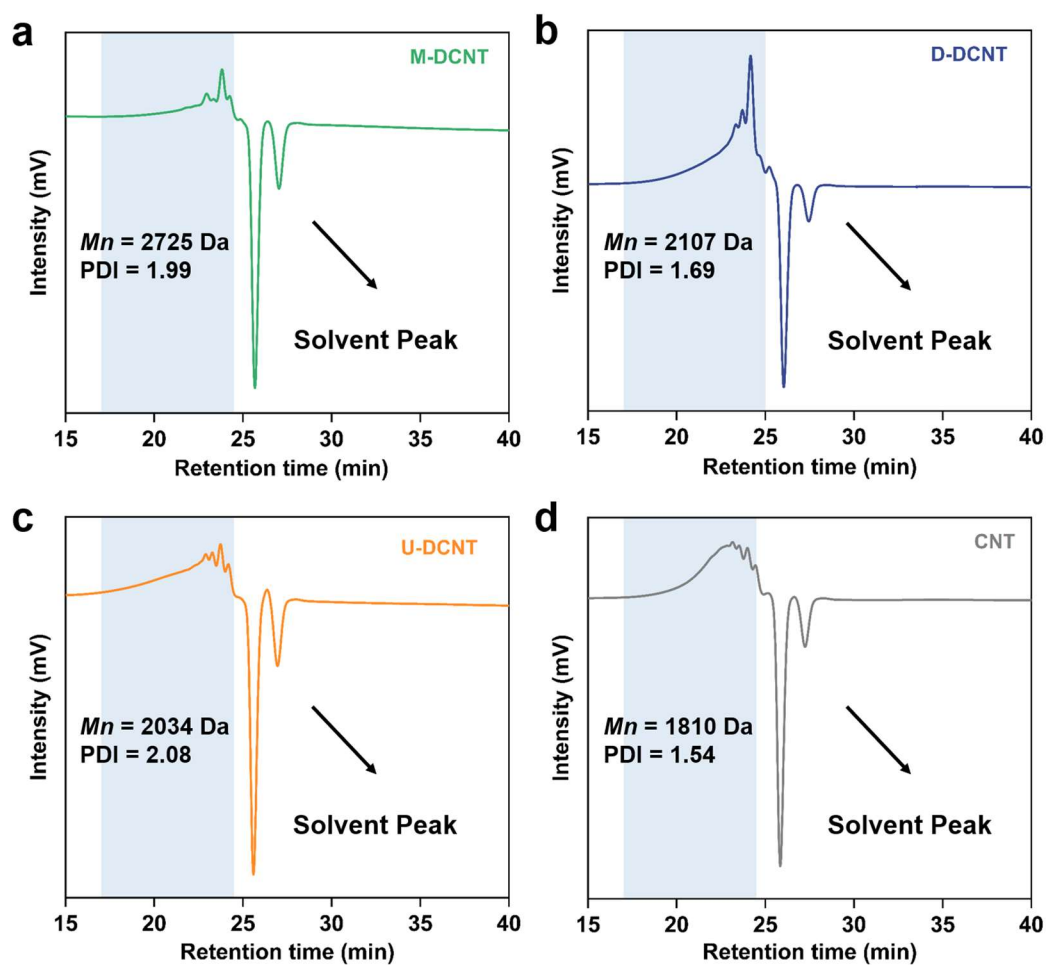


Figure S13. GPC analysis of polymerization products extracted from the surfaces of M-DCNT (a), D-DCNT (b), U-DCNT (c), and CNT (d). Reaction conditions: [Cat.] = 0.1 g L⁻¹, [PMS] = 1.0 mM, [2,6-M-PhOH] = 0.5 mM, initial pH = 7.4, and $T = 25 \pm 2^\circ\text{C}$.

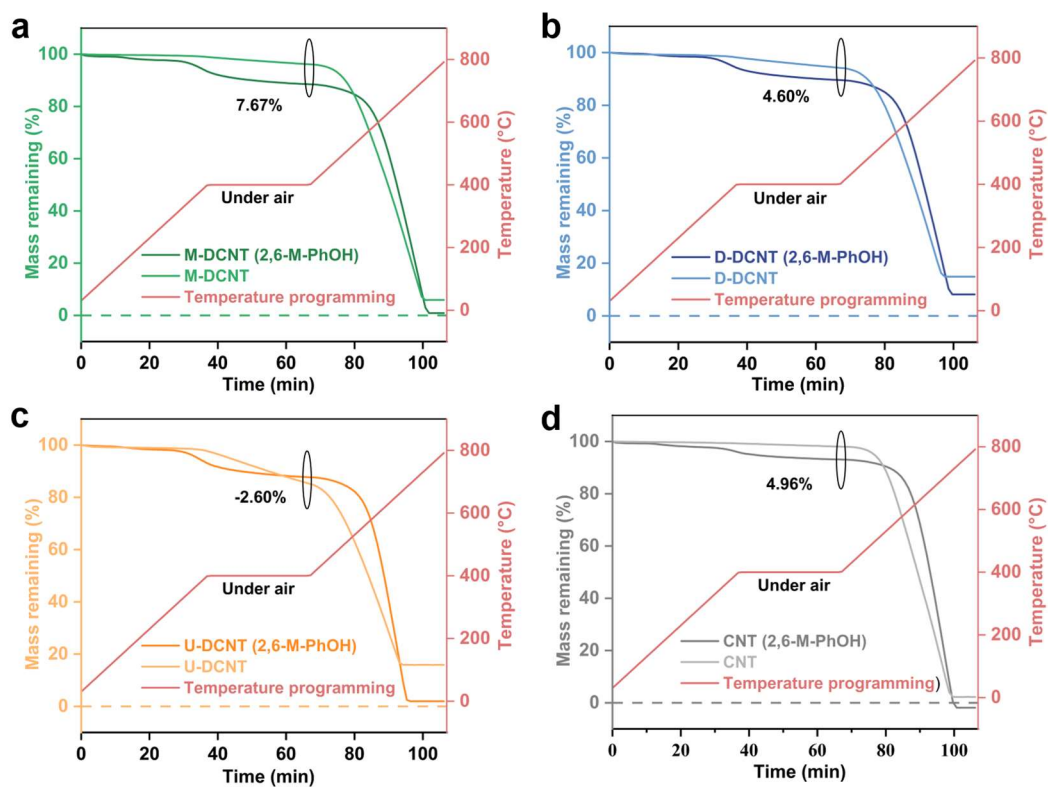


Figure S14. TGA curves of M-DCNT (a), D-DCNT (b), U-DCNT (c), and CNT (d) before and after the reaction. Reaction conditions: [Cat.] = 0.1 g L⁻¹, [PMS] = 1.0 mM, [2,6-M-PhOH] = 0.5 mM, initial pH = 7.4, and $T = 25 \pm 2^\circ\text{C}$.

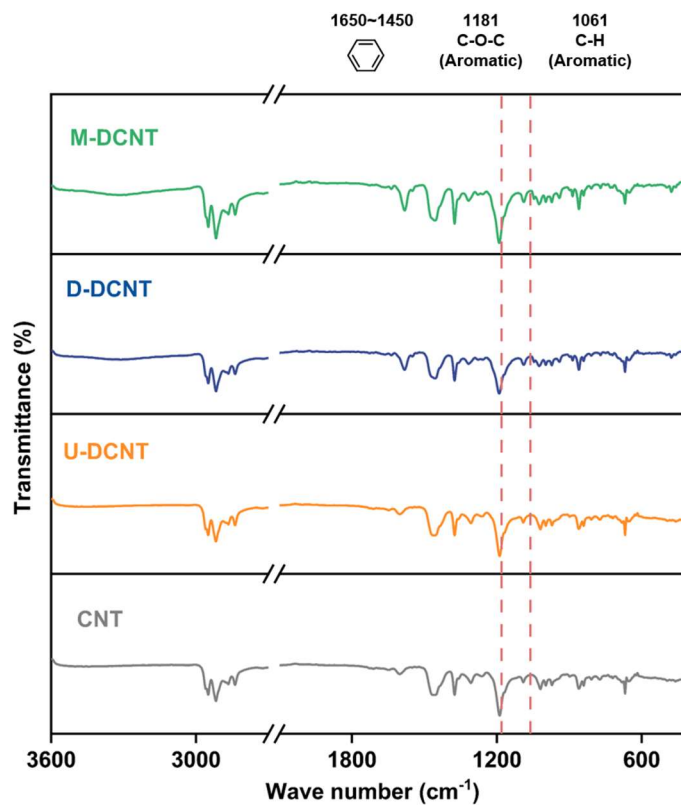


Figure S15. FTIR analysis of polymerization products extracted from M-DCNT, D-DCNT, U-DCNT, and CNT surfaces. Reaction conditions: [Cat.] = 0.1 g L⁻¹, [PMS] = 1.0 mM, [2,6-M-PhOH] = 0.5 mM, initial pH = 7.4, and $T = 25 \pm 2^\circ\text{C}$.

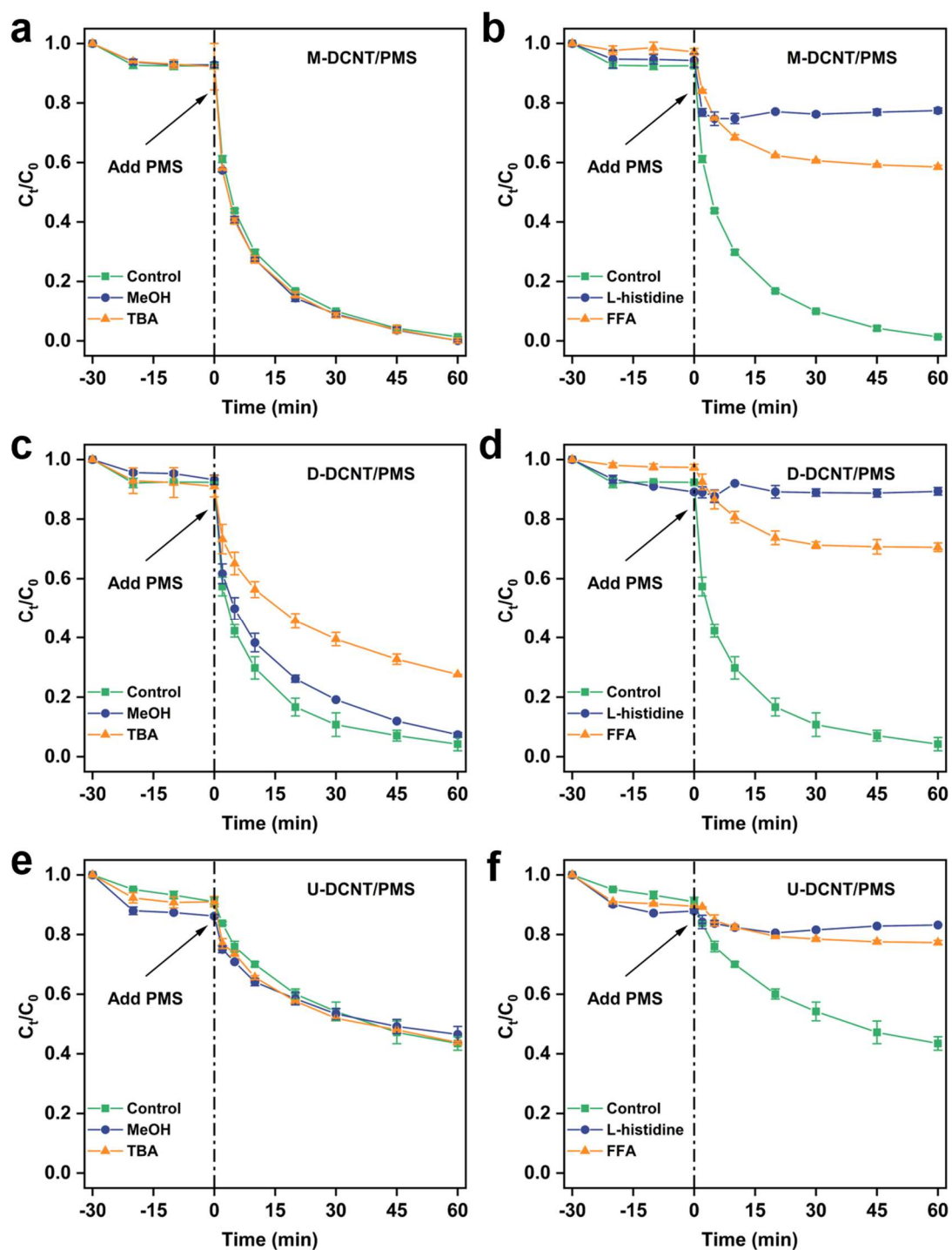


Figure S16. Quenching experiments of M-DCNT (a), D-DCNT (b), and U-DCNT (c). Reaction conditions: [Cat.] = 0.1 g L^{-1} , [PMS] = 1.0 mM , [4-CP] = 0.5 mM , [MeOH] = [TBA] = 60 mM , initial pH = 7.4, and $T = 25 \pm 2^\circ\text{C}$. The error bars represent the standard deviations from duplicate or triplicate tests.

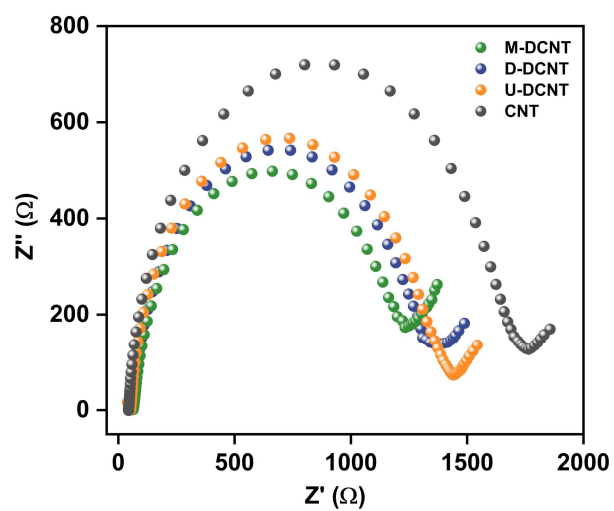


Figure S17. Electrochemical impedance spectra of M-DC NT, D-DCNT, U-DCNT, and CNT.

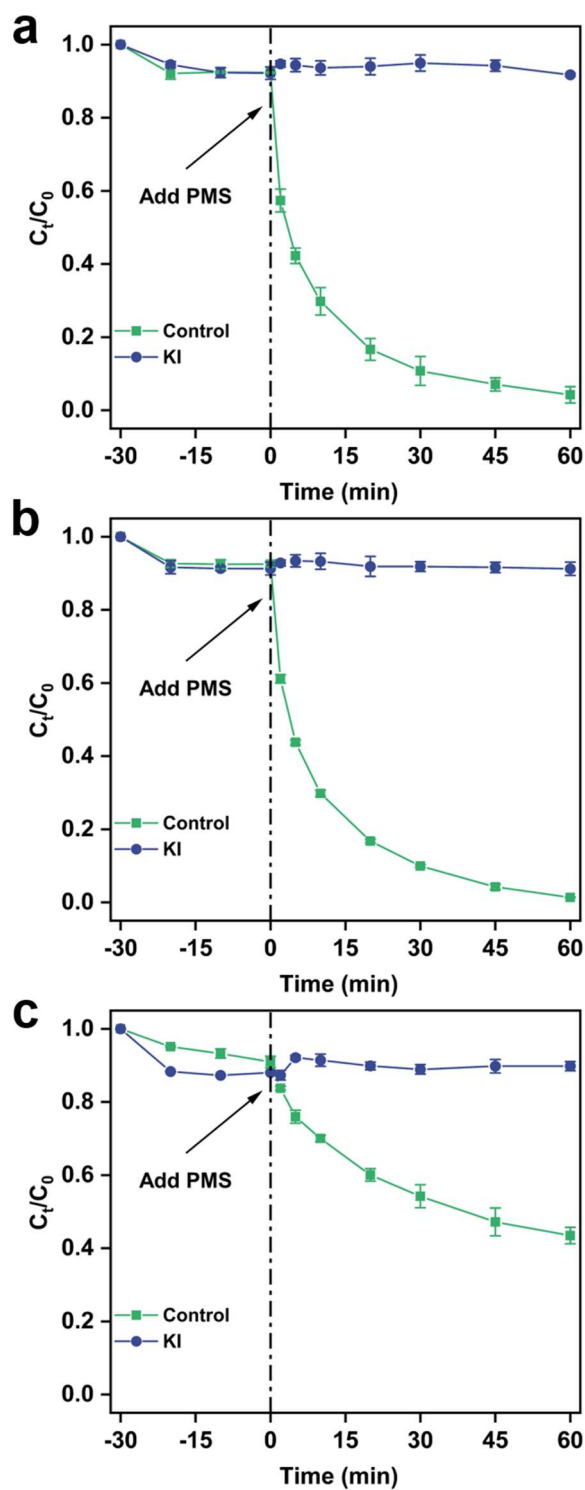


Figure S18. Quenching experiments of M-DCNT (a), D-DCNT (b), and U-DCNT (c). Reaction conditions: $[\text{Cat.}] = 0.1 \text{ g L}^{-1}$, $[\text{PMS}] = 1.0 \text{ mM}$, $[\text{4-CP}] = 0.5 \text{ mM}$, $[\text{KI}] = 6 \text{ mM}$, initial $\text{pH} = 7.4$, and $T = 25 \pm 2^\circ\text{C}$. The error bars represent the standard deviations from duplicate or triplicate tests.

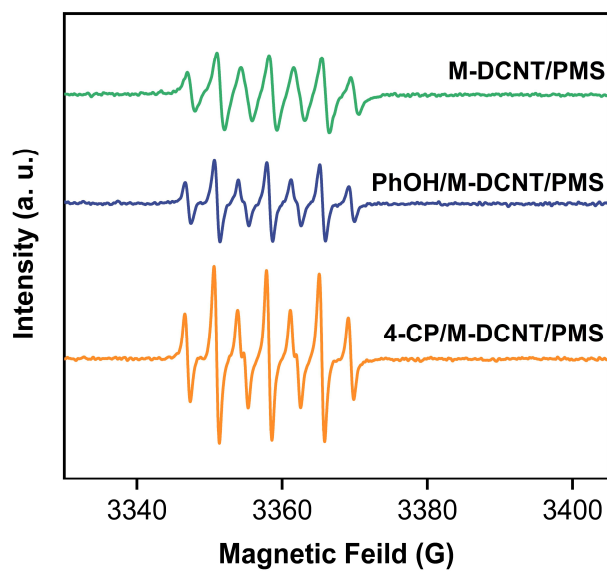


Figure S19. EPR spectra of different M-DCNT/PMS systems. Reaction conditions: [M-DCNT] = 0.1 g L⁻¹, [PMS] = 1.0 mM, [4-CP] = [PhOH] = 0.5 mM, [DMPO] = 100 mM, initial pH = 7.4, and $T = 25 \pm 2^\circ\text{C}$.

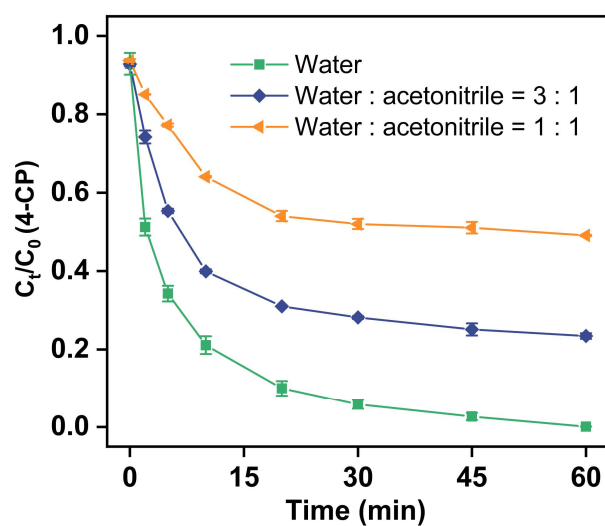


Figure S20. Competitive inhibition of acetonitrile on 4-CP removal in M-DCNT/PMS system. Reaction conditions: $[M\text{-DCNT}] = 0.1 \text{ g L}^{-1}$, $[PMS] = 1.0 \text{ mM}$, $[4\text{-CP}] = 0.5 \text{ mM}$, initial $\text{pH} = 7.4$, and $T = 25 \pm 2^\circ\text{C}$. The error bars represent the standard deviations from duplicate or triplicate tests.

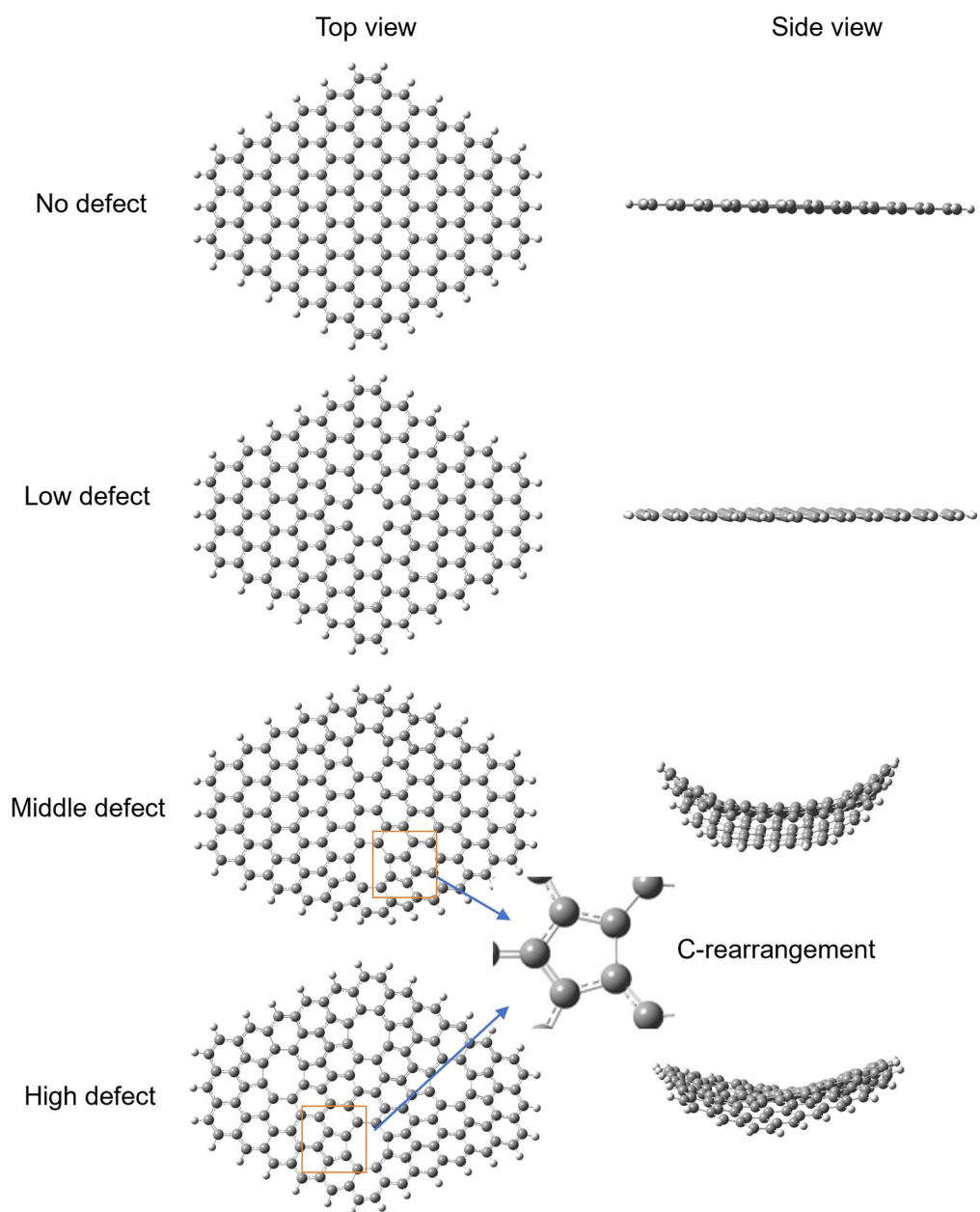


Figure S21. The constructed CNT models with different defect degrees.

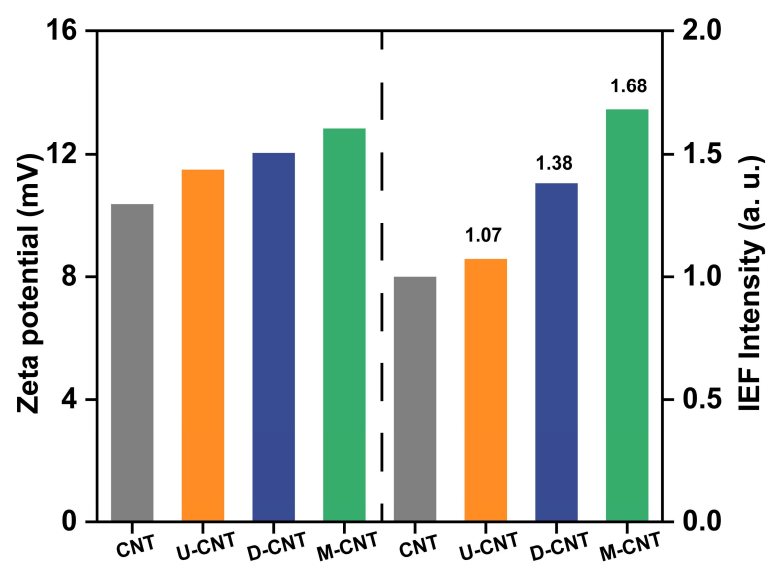


Figure S22. The comparison of Zeta potential and IEF intensity of M-DCNT, D-DCNT, U-DCNT, and CNT.

Note: All ratios are normalized here.

Reference

1. Lu, T. & Chen, F. Multiwfn: A multifunctional wavefunction analyzer. *J. Comput. Chem.* **33**, 580–592 (2012).
2. Liu, J.-Y. *et al.* Direct Electron Transfer-Driven Nontoxic Oligomeric Deposition of Sulfonamide Antibiotics onto Carbon Materials for In Situ Water Remediation. *Environ. Sci. Technol.* **58**, 12155–12166 (2024).
3. Dou, J. *et al.* Neglected but Efficient Electron Utilization Driven by Biochar-Coactivated Phenols and Peroxydisulfate: Polyphenol Accumulation Rather than Mineralization. *Environ. Sci. Technol.* **57**, 5703–5713 (2023).
4. Wei, Y. *et al.* Ultrahigh Peroxymonosulfate Utilization Efficiency over CuO Nanosheets via Heterogeneous Cu(III) Formation and Preferential Electron Transfer during Degradation of Phenols. *Environ. Sci. Technol.* **56**, 8984–8992 (2022).
5. Yue, S. *et al.* Selective Photoreforming of Waste Plastics into Diesel Olefins via Single Reactive Oxygen Species. *Angew. Chem. Int. Ed.* **63**, e202406795 (2024).
6. Li, J., Cai, L., Shang, J., Yu, Y. & Zhang, L. Giant Enhancement of Internal Electric Field Boosting Bulk Charge Separation for Photocatalysis. *Adv. Mater.* **28**, 4059–4064 (2016).
7. Wang, Z. *et al.* Cobalt Single Atoms Anchored on Oxygen-Doped Tubular Carbon Nitride for Efficient Peroxymonosulfate Activation: Simultaneous Coordination Structure and Morphology Modulation. *Angew. Chem. Int. Ed.* **61**, e202202338 (2022).

8. Huang, G.-X., Wang, C.-Y., Yang, C.-W., Guo, P.-C. & Yu, H.-Q. Degradation of Bisphenol A by Peroxymonosulfate Catalytically Activated with $\text{Mn}_{1.8}\text{Fe}_{1.2}\text{O}_4$ Nanospheres: Synergism between Mn and Fe. *Environ. Sci. Technol.* **51**, 12611–12618 (2017).
9. Khan, A. *et al.* Facile synthesis of yolk shell $\text{Mn}_2\text{O}_3@\text{Mn}_5\text{O}_8$ as an effective catalyst for peroxymonosulfate activation. *Phys. Chem. Chem. Phys.* **20**, 13909–13919 (2018).
10. Yao, Z. *et al.* High-entropy alloys catalyzing polymeric transformation of water pollutants with remarkably improved electron utilization efficiency. *Nat. Commun.* **16**, 148 (2025).
11. Huang, B.-C., Jiang, J., Huang, G.-X. & Yu, H.-Q. Sludge biochar-based catalysts for improved pollutant degradation by activating peroxymonosulfate. *J. Mater. Chem. A* **6**, 8978–8985 (2018).
12. Wu, Y. *et al.* Insights into the mechanism of persulfate activated by rice straw biochar for the degradation of aniline. *Chemosphere* **200**, 373–379 (2018).
13. Cheng, X., Guo, H., Zhang, Y., Wu, X. & Liu, Y. Non-photochemical production of singlet oxygen via activation of persulfate by carbon nanotubes. *Water Res.* **113**, 80–88 (2017).